Cytometry
PART A
Journal of the International Society for Advancement of Cytometry

Evolving Generalized Voronoi Diagrams for Accurate Cellular Image Segmentation

Weimiao Yu,[1]* Hwee Kuan Lee,[1] Srivats Hariharan,[2] Wenyu Bu,[2] Sohail Ahmed[2]

[1]Bioinformatics Institute (BII), 30 Biopolis Street, #07-01, Matrix, Singapore 138671

[2]Institute of Medical Biology (IMB), 8A Biomedical Grove #06-06, Immunos Singapore 138648

Received 29 June 2009; Revision Received 14 January 2010; Accepted 21 January 2010

*Correspondence to: Weimiao Yu, 30 Biopolis Street, #07-01 Matrix, Singapore 138671

Email: yuwm@bii.a-star.edu.sg

Additional Supporting Information may be found in the online version of this article.

Published online 18 February 2010 in Wiley InterScience (www.interscience.wiley.com)

DOI: 10.1002/cyto.a.20876

Abstract

Analyzing cellular morphologies on a cell-by-cell basis is vital for drug discovery, cell biology, and many other biological studies. Interactions between cells in their culture environments cause cells to touch each other in acquired microscopy images. Because of this phenomenon, cell segmentation is a challenging task, especially when the cells are of similar brightness and of highly variable shapes. The concept of topological dependence and the maximum common boundary (MCB) algorithm are presented in our previous work (Yu et al., Cytometry Part A 2009;75A:289–297). However, the MCB algorithm suffers a few shortcomings, such as low computational efficiency and difficulties in generalizing to higher dimensions. To overcome these limitations, we present the evolving generalized Voronoi diagram (EGVD) algorithm. Utilizing image intensity and geometric information, EGVD preserves topological dependence easily in both 2D and 3D images, such that touching cells can be segmented satisfactorily. A systematic comparison with other methods demonstrates that EGVD is accurate and much more efficient. © 2010 International Society for Advancement of Cytometry

Key terms

image cytometry; cell segmentation; fluorescence microscopy; generalized Voronoi diagram

ANALYZING cellular morphology is crucial in drug discovery, cell and developmental biology. Automated high-content image-based approaches are preeminent tools, which enable thousands of images to be acquired. However, acquiring high quality images is only the first step towards biological discoveries. Image processing—computer-based interrogation is essential to extract useful data from the images acquired. To extract the quantitative information on a cell-by-cell basis, a critical but challenging task is to segment individual cells. Once cells have been segmented successfully, subsequent analysis including cell counting, morphology, and migration becomes possible.

In the images acquired by high-content screening experiments, the cells can be classified into three groups; (i) isolated, (ii) touching, and (iii) overlapping. In monolayer cell cultures, as shown in Figure 1, isolated cells are the cells that are well separated from other cells, touching cells are the cells that adhere to other cells and share some common boundaries, and overlapping cells are the cells that lie on top of each other with no clear boundary. Touching cells form the majority of cells in normal culture conditions. Segmentation of the isolated cells is straightforward as simple thresholding can successfully segment them, while segmentation of the touching cells is much more challenging.

Among many existing cell segmentation approaches, active contours represented through the level set is a successful way to segment cells of irregular shapes. The Mumford–Shah model (1) is proposed to segment two-phase piecewise constant images. This model is enhanced by Chan–Vese (2) using the level set concept introduced in (3). However, the level set formulation lacks the ability to constrain

ISAC
International Society for Advancement of Cytometry

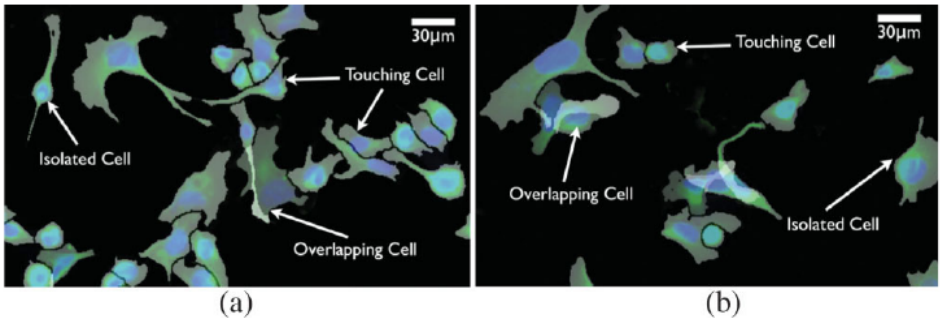

Figure 1. Illustration of isolated cells, touching cells and overlapping cells. HP Pavilion TX2500 and Photoshop CS3 extended are used to label the ground truth. The ground-truth segments are shown by the transparent white masks.

topological changes, for example, splitting and merging. In practice, this limitation fosters undesired merging of segments of touching cells due to similar gray level intensity.

To overcome this limitation, one popular solution is to use multiple level set functions for multiple cells. A multiphase level set model is presented in (4), in which $\log_2(n)$ level set functions are applied to represent n phases. Each phase represents a number of cells of similar brightness. However, this approach again cannot segment cells satisfactorily as it does not penalize overlapping and merging of touching cells with similar brightness. To overcome this problem, different coupling terms (5–7) are added into Mumford–Shah function. The additional coupling terms penalize overlapping and merging of different cells. The minimization of modified function including the coupling terms can separate the cells. Using this idea, n level set functions are applied to segment n cells in 2D (5,6) and 3D (7). Utilization of multiple level set functions for multiple cells is computationally expensive when the number of cells increases. As thousands of images are acquired in high-throughput experiments, algorithm speed is an important consideration. A significant improvement is the four-color level set algorithm (8). Using the Delaunay graph to capture spatial relationship of cells and reducing the complexity of the coupling constraint dramatically reduces the computational cost.

To distinguish different touching cells, another popular solution is to determine the topology of cells and then apply topological constraints. The watershed approach is a common method to preserve the predetermined topology in combination with level set (9). However, over-segmentation is a well-known issue of the watershed approach. Some approaches have been reported to circumvent this problem, for example, rule-based merging (10), marker-controlled watershed correction (11), and gradient-based region growth (12). Besides watershed approaches, other topology preserving approaches are also proposed. Using the simple point concept (13), topology is preserved by checking the topological number, connectivity, and sign change of each point during the level set evolution. Another topology-preserved model (14) is based on the minimization of a complex function within a narrow band around the zero level set.

In many biological experiments, nuclei images are usually acquired using an independent channel. The segmented nuclei can be used to determine the topology of the cells and serve as references. Different 2D nuclei segmentation methods have been reported, such as simple thresholding (15), watershed algorithm (16,17), level set boundary searching using gradient flow (18), active contour model for closely packed nuclei (19–21), and ellipse detection algorithm (22). A few 3D nuclei segmentation approaches (23,24) are recently reported as well.

Using classical level set formulation without special treatments or topological constraints, two or more distinct touching cells will be segmented as one single object. In our previous work (25,26), we presented a simple concept, topological dependence, to segment the touching cells. The undesired topological changes are prevented using the maximum common boundaries (MCB) criterion, which is a kind of rule-based merging method. Although our results showed that topological dependence is an efficient constraint to segment touching cells, the MCB algorithm still has room for improvement. Three limitations of MCB are highlighted below.

(a) Algorithm efficiency is a key consideration for high-throughput screening experiments and computational effort of MCB becomes high as cell number increases.
(b) The generalization of topological dependence using MCB algorithm from 2D to 3D is difficult, since it requires advanced integration algorithms to calculate the arbitrary physical area of common surfaces.
(c) The implementation of MCB is difficult as we have to consider various cases in which the level set function splits and merges.

In this article, we present a novel algorithm called evolving generalized Voronoi diagram (EGVD), which overcomes the (a)–(c) limitations mentioned earlier. In particular, for high throughput screening, the EGVD approach substantially improves the computational speed.

Materials and Methods

Cell Culture

N1E115 is a mouse neuroblastoma cell line model for neurons and has been used to study the morphological roles

of Rho GTPases and effectors in Refs. 27–29. We chose N1E115 cells as our model as they have the potential to develop complicated morphology when they differentiate into neurons induced by serum starvation or the transfection of transducer of Cdc42-dependent actin assembly (Toca-1). Toca-1 was first identified as an essential component of Cdc42 mediated actin polymerization using *Xenopus* extract (30). The phenotype of Toca-1 transfected cells was multiple branching neurites with filopodia (26,31). Quantitative morphology comparisons of serum starvation and Toca-1 transfection are reported in (26). A more complete study on the cellular functions of Toca-1 is presented in (31). In our study, cellular images were acquired under four culture conditions: (i) Serum starvation with 50,000 cells/slide; (ii) Serum starvation with 30,000 cells/slide; (iii) Toca-1 transfected with 50,000 cells/slide; (iv) Toca-1 transfected with 30,000 cells/slide. The images in our experiment contain both undifferentiated cells of regular shape and differentiated cells of complicated morphology.

N1E115 cells are maintained in 90 mm cell culture dish at 37°C in a humidified atmosphere supplied with 5% CO_2. The culture medium is Dulbecco's modified Eagle's medium with 4,500 mg/ml glucose supplemented with 10% fetal bovine serum and 1% penicillin–streptomycin as antibiotic. Then the cells were seeded onto 18 mm × 18 mm glass coverslip coated with 10 μg/ml laminin at appropriate densities 24 h before Toca-1 transfection. Laminin is an extracellular matrix protein used to coat the coverslip before seeding. Cells were then washed with fresh warm medium and resuspended at appropriate densities. For Condition (i) and (ii), the cells were serum starved for 48 h. For Condition (iii) and (iv), Toca-1 was transfected into N1E115 cells using Lipofectamine2000 (Invitrogen) and proteins expressed for 24–36 h before fixation. Transfection here stands for the method to effectively deliver plasmid DNA (Toca-1) into the cells. Twenty-four hours after transfection, the cells were washed three times with phosphate buffered saline (PBS) and incubated in 300 nM DAPI (Molecular Probe) for 5 min. The cells then rinsed in PBS several times and fixed in 4% paraformaldehyde at room temperature for 15 min.

Image Acquisition

The cellular images are acquired from the N1E115 cells prepared as earlier. The cells are stained by DAPI and FITC-phalloidin. DAPI is a blue dye that stains double strand DNA in nucleus. FITC-phallodin stains the abundant filamentous actin, which visualized as green. The cells are counted, seeded, and resuspended into monolayer cultures on coverslips with a density of 50–70% confluency. The seeding procedure guarantees that nuclei do not overlap with each other. We use a motorized, inverted Zeiss Aviovert 200 microscope with filters for DAPI and FITC to acquire the images. The system includes a motorized XY stage, CoolSnapHQ CCD camera, and an external motorized fluorescence filter wheel for rapid imaging. Image acquisition is controlled by Metamorph[1] software. We used the Zeiss Plan-Apochromat 20×/0.8 objective lens for imaging. Exposure time for DAPI was set at 50 ms and for FITC at 100 ms. Camera Binning was set at 1 × 1. Read out speed from the camera was 20 MHz. Image formats were 1392 × 1040 pixels and of 12 bits accuracy. Each pixel was 0.3 μm × 0.3 μm. The entire coverslip (18 mm × 18 mm) was scanned and ~1,500 images for each condition were acquired.

[1]http://www.moleculardevices.com/pages/software/metamorph.html.

Evolving Generalized Voronoi Diagram (EGVD)

In our previous work (26), we proposed a simple but efficient concept, topological dependence, to segment touching cells by using MCB criteria. However, MCB suffers a few drawbacks as discussed in Section 1. Here, we present a simpler and faster algorithm, EVGD, to preserve the topological dependence. The details of the MCB approach and definitions for topological dependence, level set function initialization, evolution and parameter selection can be found in our previous papers (25,26). Topological dependence simply tells us that each cell contains exactly one nucleus and it must be inside of the cell. In the rest of this article, we use $\omega_i^{c,t}$ to denote the cell segments at artificial time t and use ω_i^n to denote the segmented nuclei. When $t = 0$, we have $\omega_i^{c,t=0} = \omega_i^n$, which means that initially each cell segment is topologically dependent with nuclei segment ω_i^n (25,26). Before presenting our algorithm, let's first introduce two definitions.

Generalized Voronoi Diagram

Given a set of disjoint path-connected regions $\omega_i^{c,t}$ for $i = 1,2,\ldots,L$ with $\omega_i^{c,t} \cap \omega_j^{c,t} = \emptyset \ \forall \ i \neq j$, define the generalized Voronoi diagram (GVD) (32) as $V_i(\omega_1^{c,t}, \omega_2^{c,t}, \ldots, \omega_L^{c,t})$ corresponding to each $\omega_i^{c,t}$:

$$V_i(\omega_1^{c,t},\omega_2^{c,t},\ldots,\omega_L^{c,t}) = \left\{ r \in \Theta \,|\min_{s\in\omega_i^{c,t}} |r-s| < \min_{s'\in\bigcup_{j\neq i}^{L}\omega_j^{c,t}} |r-s'| \right\} \quad (1)$$

Selector

Given a connected region ω_i^n and a set of connected regions Γ. Defined the Selector, also known as choice function (33), S $(\Gamma|\omega_i^{c,t})$ that selects one connected region from Γ, which contains ω_i^n.

Instead of an impolitic "cutting and pasting" approach of MCB algorithm, topological dependence is preserved more easily and efficiently using EGVD algorithm. Our segmentation consists of two loops of iterations. The outer loop is for the level set evolution and the inner loop is to evolve GVD. The algorithm is given as follows:

EGVD Algorithm

1. Segment the nuclei to obtain ω_i^n, $i = 1,2,\ldots,L$ as in Refs. 25 and 26 or using other approaches.
2. Transform f^c and initialize the level set function for the cell segmentation (25,26) to obtain the initial cell segments $\omega_i^{c,t=0}$.

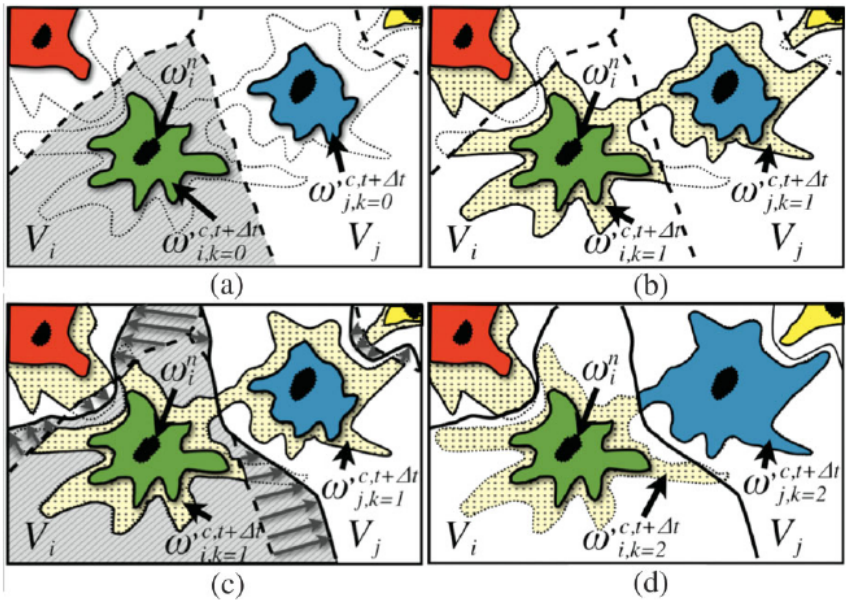

Figure 2. Illustration of evolving generalized Voronoi diagram and topological dependence. The shaded regions in (**a**) and (**c**) are corresponding V_i for $\omega_{i,k=1}^{\prime c,t+\Delta t}$ and $\omega_{i,k=2}^{\prime c,t+\Delta t}$. The dotted regions represent the different $\omega_{i,k}^{\prime c,t+\Delta t}$ at different iterations before convergence. The arrows in (**c**) show how the boundaries of GVD are evolving and stretching.

3. Update the level set function $\phi_t^c \rightarrow \phi_{t+\Delta t}^c$ according to Refs. 25 and 26. Then iteratively update the GVD regions at each time step $t + \Delta t$ to obtain $\omega_i^{c,t+\Delta t}$:
   (a) Let $\Omega^{c,t+\Delta t} = \{r \in \Theta \mid \phi_{t+\Delta t}^c(r) \geq 0\}$.
   (b) Define $\omega_{i,k=0}^{\prime c,t+\Delta t} = \omega_i^{c,t}$, for $i = 1,2,\ldots,L$. k is the index of successive estimates of cell segments at $t + \Delta t$.
   (c) For each $i = 1,2,\ldots,L$, calculate the GVD, $V_i(\omega_{1,k}^{\prime c,t+\Delta t}, \omega_{2,k}^{\prime c,t+\Delta t}, \ldots, \omega_{L,k}^{\prime c,t+\Delta t})$, given by Eq. (1). Then update the cell segment using Selector:

$$\omega_{i,k+1}^{\prime c,t+\Delta t} = S(\Omega^{c,t+\Delta t} \cap V_i(\omega_{1,k}^{\prime c,t+\Delta t}, \omega_{2,k}^{\prime c,t+\Delta t}, \ldots \omega_{t..k}^{\prime c,t+\Delta t}) | \omega_i^n) \quad (2)$$

   (d) Iterate step 3(c) until convergence, that is, $\omega_{i,k+1}^{\prime c,t+\Delta t} = \omega_{i,k}^{\prime c,t+\Delta t}$
   (e) Set $\omega_i^{c,t+\Delta t} \leftarrow \omega_{i,k+1}^{\prime c,t+\Delta t}$.
4. Repeat step 3 until the convergence of level set function.

A proof of the convergence for this algorithm is given in the Supporting Information. We give an intuitive example using Figure 2. GVDs shown by the shaded regions in Figures 2a and 2c define the boundaries of cell segments where they might merge. Initially, topological dependence between $\omega_i^{c,t}$ and ω_i^n is satisfied at time t and the boundaries of the GVD are indicated by the dashed lines in Figure 2a. At time $t + \Delta t$, the level set function is updated and some objects might merge, illustrated by the regions enclosed by dotted outline. The GVD calculated at the previous time step t is used as initial GVD for the inner loop iteration. Given GVD and ω_i^n, the Selector will choose a connected region for each cell, shown by the dotted regions in Figure 2b. Then a new GVD is calculated based on these connected regions, as shown by the shaded area in Figure 2c. The arrows in Figure 2c show how boundaries of GVD are evolved and stretched. The process of evolving GVD is performed iteratively until GVD does not change anymore.

Results

Two original images and their segmentation results using EGVD algorithm are shown in Figure 3. The cells are crowded and touching each other. Nevertheless, the EGVD algorithm can segment individual cells correctly.

Ground Truth and Validation

To quantitatively validate our algorithm, we randomly selected 100 images containing 4,983 cells (25 images from each condition) to create the ground truth. The ground truth is manually segmented, according to human perception. In Figure 1, the ground-truth segments are overlaid with the original images. We use the ground truth to compare the performances of Metamorph Ver7.0r4, CellProfiler (34), MBC algorithm (25,26), and EGVD algorithm. In MetaMorph, three parameters were carefully tuned to optimize data analysis. The parameters are approximate max cell width (30 μm), intensity above local background (100), and minimum cell area (50 μm^2). The parameters used for CellProfiler are those suggested by its author (personal correspondence).

We defined a score α_i to describe the accuracy of our segmentation. Let $\omega_j^g j = 1,2,\ldots,N$ be the ground-truth segments and $\omega_i^s i = 1,2,\ldots,M$ be the computational segments, as shown

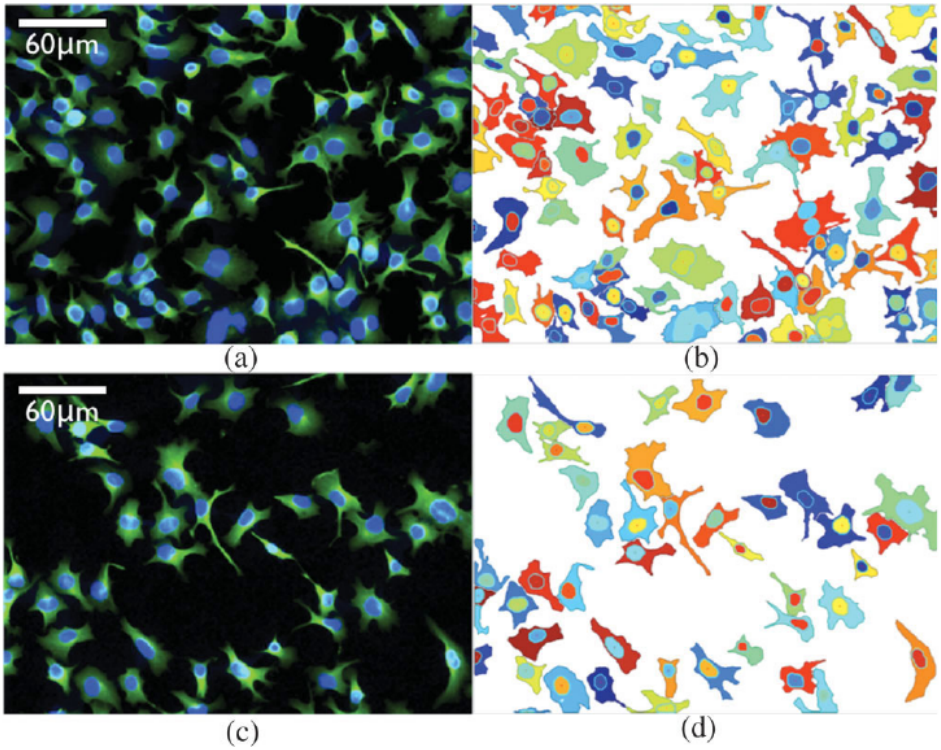

Figure 3. Original images and the segmented images. (**a**) and (**c**) are the original images, (**b**) and (**d**) are the segmented images. Although the cells are touching each other, EGVD algorithm is able to segment individual cells correctly.

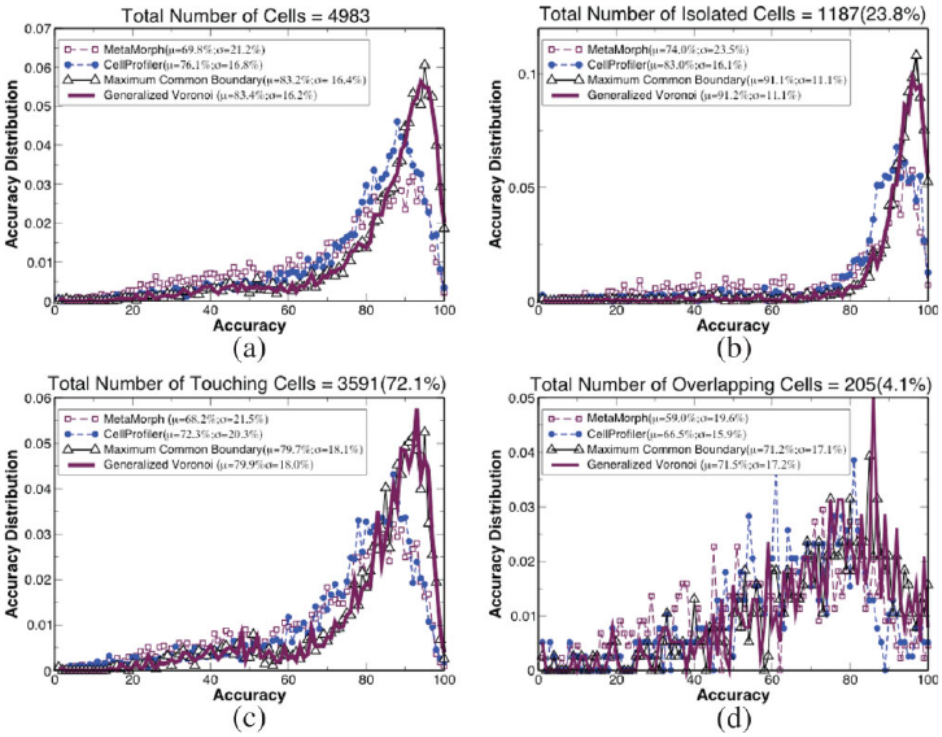

Figure 4. Results comparison between MetaMorph, CellProfiler, maximum common boundary and evolving generalized Voronoi diagram. (**a**) The accuracy distribution for all cells; the performance of both our approach is better than MetaMorph and CellProfiler. (**b**), (**c**), (**d**) show the accuracy distribution of isolated cells, touching cells, and overlapping cells, respectively. The populations of the touching cells are majority of the cells and the overlapping cells are only 4.1%. The improvement of our approaches over MetaMorph and CellProfiler for isolated cells and touching cells are clear. None of the given four approaches can segment the overlapping cells satisfactorily.

Table 1. Statistics of different segments of four different approaches

	META MORPH	CELLPROFILER	MCB	EGVD
Matched segments	4,989 (96.26%)	4,656 (93.34%)	4,912(98.58%)	4,911 (98.56%)
Unmatched GT segments	194 (3.74%)	327 (6.56%)	71 (1.42%)	72 (1.44%)
Unmatched segments	0 (0.00%)	5 (0.10%)	0 (0.00%)	0 (0.00%)

in Figure 4a. (i) We calculate an accuracy score α_i for each computational segment ω_i^s:

$$\alpha_i = \max_j \left(\frac{|\omega_i^s \cap \omega_j^g|}{|\omega_i^s \cup \omega_j^g|} \right) \quad (3)$$

where $|\cdot|$ means to calculate the area. The score is the ratio between the area of $\omega_i^s \cap \omega_j^g$ and $\omega_i^s \cup \omega_j^g$. Given a computational segment, α_i will have a value between 0 (totally wrong) and 1.0 (perfect segment). If ω_i^s does not overlap with any ω_j^g, $\alpha_i = 0$. We call those segments as Unmatched Segments. On the other hand, if ω_j^g does not overlap any ω_i^s, we call those ground-truth segments as Unmatched GT Segments. Table 1 shows that both EGVD and MCB have less Unmatched GT segments. The number of Unmatched Segments can be ignored for all four approaches.

We calculated the score α_i for each segmented cells using these four approaches. The distributions of α_i are shown in Figure 4a. The performance of EGVD algorithm is slightly better than MCB algorithm as they are both under the same topological constraint. The mean accuracies of both approaches are about 7% higher than CellProfiler and 13% higher than MetaMorph. As discussed in Section 1, there are generally three types of cells, for example, isolated cell, touching cell, and overlapping cell. As shown in Figure 4b, the isolated cells are only 23.8% of the total cells in our data set and the mean accuracies of our approaches for isolated cells are about 8% and 17% higher than CellProfiler and MetaMorph. The touching cells form the majority, at about 72.0% and Figure 4c shows the distributions of α_i of this population. For the touching cells, the mean accuracies of our approaches are 8 and 12% higher than CellProfiler and MetaMorph, respectively. Figure 4d shows that the overlapping cells are only a small population. None of the four approaches could solve the problem of overlapping cells satisfactorily.

We analyzed how the cell density of the image (cell number/image, Fig. 5a) affects cell populations. As shown in Table 2, the cell density significantly affects the percentages of isolated cells, touching cells, and overlapping cells. For example, Condition (i) has the highest cell density (94 cells/image) contains 80.9% touching cells. Condition (iii) has the lowest cell density (26 cells/image) contains only 56.0% touching cells.

The efficiency of the algorithm is an important consideration in high-throughput screening experiments. We compared the computational time of EGVD algorithm and MCB algorithm. As shown in Figure 5b, the EGVD approach is much more efficient when the number of the cells is large and the analysis contains more touching cells. The slope of linear fitting for the computational time versus the number of cells is 0.16 for EGVD and 0.43 for MCB. This means that the EGVD is approximately three-fold faster than MCB.

Discussion

Accurate cell segmentation is a prerequisite to extract cell-by-cell information for cell biology studies. One of the major challenges here is how to segment touching cells, which sometimes have highly variable morphology. In this article, we present the EGVD algorithm as a means to preserve the topological dependence introduced in Refs. 25 and 26. Topological dependence is essential to ensure satisfactory cell segmentation and the EGVD algorithm preserves this constraint more easily and efficiently. To test the EGVD we created a ground

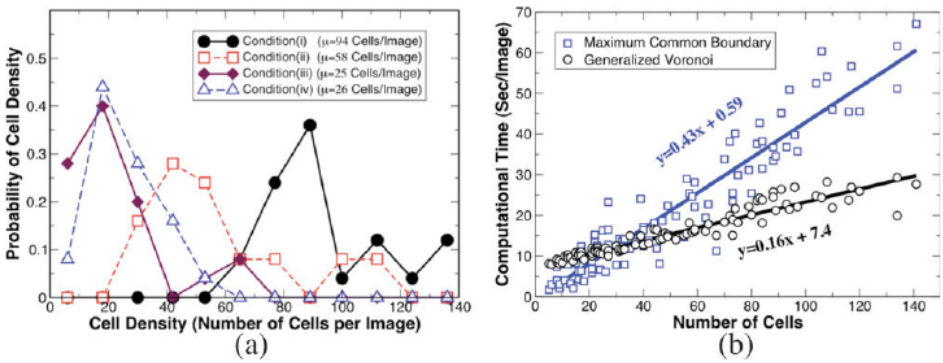

Figure 5. Cell density and the comparison of computational time of maximum common boundary (MCB) and evolving generalized Voronoi diagram (EGVD). (**a**) The distributions of cell density under different conditions. (**b**) The computational time for MCB and EGVD. EGVD reduced the computational time significantly for the images containing more cells. The computational time is also very consistent.

Table 2. Cell density, number and percentage of different types of cells based on 4983 ground truth segments under different culture conditions

	CONDITION (I)	CONDITION (II)	CONDITION (III)	CONDITION (IV)
Cell density (Cell/Image)	94	58	25	26
Isolated cells	15.4%	26.0%	35.1%	40.1%
Touching cells	80.9%	71.0%	55.9%	56.0%
Overlapping cells	3.7%	3.0%	9.0%	3.9%

truth[2] manually for 100 randomly selected images containing 4,983 cells. Our result shows that the touching cells are the majority (>70%) in these images. Based on our calculation, EGVD is three-fold faster than MCB for these images and this improvement is essential for the high-throughput screening experiments.

Compared with existing approaches EGVD has a number of distinct advantages.

(i) Instead of using multiple level set function for multiple cells (4–8), EGVD requires only one level set function to segment all cells. The introduction of the coupling terms (5–8) or imposing topology constraint on a narrow band of level set (14) can prevent the merging, however, the hyper-parameters, which control the penalization of overlapping, need to be determined empirically or computationally.

(ii) In the MCB algorithm, the topological dependence is preserved by awkward "cutting and pasting" while with EGVD the spatial connectivity of cell segments and topological dependence are appropriately preserved. It is not necessary to check the topological number and sign change of each point during every iteration as in Ref. 13. The formulation in Ref. 14 disallows any topological change while EGVD only requires path connectivity and is thus more flexible. For example, EGVD allows adding a hole into a simple connected segment.

(iii) The generalization of topological dependence using the MCB algorithm, for example, from 2D to 3D, is very difficult as it requires advanced integration algorithms, meshing and surface fitting techniques to calculate the arbitrary physical area of common surfaces. In contrast, EGVD is conceptually simple and straightforward to implement as it does not care about the length/area of the common boundaries/surfaces. Using EGVD, the generalization of topological dependence to higher dimensions also becomes straightforward. We have applied the EGVD approach successfully to neural stem cell segmentation in free-floating 3D aggregates of cells known as neurospheres. The details for use of the EVGD in 3D segmentation of neurospheres are being written-up and will be published in due course. However, to demonstrate the utility of the EGVD in 3D, we present three videos in the online Supporting Information.

We have consolidated the EGVD algorithm into our NeuronCyto V2.0 package with a designed user-friendly graphics interface. This package can automatically quantify and analyze the neurites in the microscopy images. The user manual for this package can be found in the Supporting Information. Both the source code of the EGVD algorithm and the NeuronCyto V2.0 package with the interface are available online at http://neuroncyto.bii.a-star.edu.sg.

[2]Our ground-truth database is available at ftp://ccdb.ucsd.edu/YU/GroundTruth.zip. The original RGB images of 8-bit are available at ftp://ccdb.ucsd.edu/YU/Original%208_Bit.zip.

Acknowledgments

The authors thank Dr. Anne E. Carpenter who provided the parameters of CellProfiler based on our images. The authors also thank Dr. Maryann Martone, Dr. Amarnath Gupta, and Dr. Mark Ellisman for hosting our ground-truth dataset on the Cell Centered Database (CCDB).

Literature Cited

1. Mumford D, Shah J. Optimal approximations by piecewise smooth functions and associated variational problems. Community Pure Appl Math 1989;42:577–685.
2. Chan TF, Vese LA. Active contours without edges. IEEE Trans Image Process 2001;10:266–277.
3. Stanley O, Sethian JA. Fronts propagating with curvature-dependent speed: Algorithm based on hamilton-jacobi formulation. J Comput Phys 1998;79:12–49.
4. Vese LA, Chan TF. a multiphase level set framework for image segmentation using mumford and shah model. Int J Comput Vis 2002;50:271–293.
5. Zhang B, Zimmer C, Olivo-Marin J-C. Tracking fluorescent cells with coupled geometric active contours. IEEE Int Symp Biomed Imaging: Nano to Macro 2004;1:476–479.
6. Yan P, Zhou X, Shah M, Wang STC. Automatic segmentation of high-throughput RNAi fluorescent cellular images. IEEE Trans Inf Technol Biomed 2008;12:109–117.
7. Dufour A, Shinin V, Tajbakhsh S, Guillen-Aghion N, Olivo-Marin JC, Zimmer C. Segmenting and tracking fluoresent cells in dynamic 3d microscopy with coupled active surfaces. IEEE Trans Image Process 2005;14:1396–1410.
8. Nath SK, Palaniappan K, Bunyak F. Cell Segmentation Using Coupled Level Sets and Graph-Vertex Coloring. Medical Image Computing and Computer-Assisted Intervention, Lect Notes Comput Sci 2006;4190:101–108.
9. Tai X, Hodneland E, Weickert J, Bukoreshtliev NV, Lundervold A, Gerdes H. Level set methods for watershed image segmentation. Lect Notes Comput Sci 2007;4485:178–190.
10. Wählby C, Lindblad J, Vondrus M, Bengtsson E, Bjorkesten L. Algorithm for cytoplasm segmentation of fluorescent labeled cells. Anal Cell Pathol 2002;24:101–111.
11. Zhou X, Liu KY, Bradblad P, Perrimon N, Wang STC. Towards automated cellular image segmentation for RNAi genome-wide screening. In: Duncan, Gerig G, editors. Proceeding of Medical Image Computing and Computer Assisted Intervention. Palm Springs, CA. 2005. pp 885–892.
12. Fenistein D, Lenseigne B, Christophe T, Brodin P, Genovesio A. A fast, fully automated cell segmentation algorithm for high-throughput and high-content screening. Cytometry Part A 2008;73A:958–964.
13. Xiao H, Chenyang X, Jerry LP. A topology preserving deformable model using level sets. Proc IEEE Comput Soc Conf Comput Vis Pattern Recognit 2001;2:765–770.
14. Le Guyader C, Vese LA. Self-repelling snake for topology-preserving segmentation models. IEEE Trans Image Process 2008;17:767–779.
15. Lerner B, Clocksin WF, Dhanjal S, Hulten MA, Christopher MB. Automatic signal classification in fluorescence in-situ hybridisation images. Bioimaging 2001;43:87–93.
16. Lockett SJ, Herman B. Automatic detection of clustered, fluorescence-stained nuclei by digital image-based cytometry. Cytometry 1994;17:1–12.
17. Malpica N, Solorzano de CO, Vaquero JJ, Santos A, Vallcorba I, Garcia-Sagredo J, Pozo del F. Applying watershed algorithms to the segmentation of clustered nuclei. Cytometry 1997;28:289–297.
18. Solorzano de CO, Malladi R, Lelievre SA, Lockett SJ. Segmentation of nuclei and cells using membrane related protein markers. J Microsc 2001;201:404–415.
19. Clocksin WF. Automatic segmentation of overlapping nuclei with high background variation using robust estimation and flexible contour model. Proc 12th Int Conf Image Anal Process 2003;17:682–687.
20. Hu M, Ping X, Ding Y. Automated cell nucleus segmentation using improved snake. Proc Int Conf Image Process 2004;4:2737–2740.

21. Murashov DM. A two-level method for segmenting cytological images based on active contour model. Pattern Recognit Image Anal 2008;18:177–192.
22. Yap CK, Lee HK. Identification of cell nucleus using a Mumford–Shah ellipse detector. Adv Visual Comput Lect Notes Comput Sci 2008;5358:582–593.
23. Gertych A, Wawrowsky KA, Lindsley E, Vishnevsky E, Farkas DL, Tajbakhsh J. Automated quantification of DNA demethylation effects in cells via 3D mapping of nuclear signatures and population homogeneity assessment. Cytometry Part A 2009; 75A:569–83.
24. Vermolen BJ, Garini Y, Young IT, Dirks RW, Raz V Segmentation and analysis of the three-dimensional redistribution of nuclear components in human mesenchymal stem cells. Cytometry Part A 2008;73A:816–824.
25. Yu WM, Lee HK, Hariharan S, Bu WY, Ahmed S. Level set segmentation of cellular images based on topological dependence. Int Symp Vis Comput Lect Notes Comput Sci 2008;5358:540–551.
26. Yu WM, Lee HK, Hariharan S, Bu WY, Ahmed S Quantitative neurite outgrowth measurement based on image segmentation with topological dependence. Cytometry Part A 2009;75A:289–297.
27. Kozma R, Ahmed S, Best A, Lim L. The GTPase-activating protein n-chimaerin cooperates with Rac1 and Cdc42Hs to induce the formation of lamellipodia and filopodia. Mol Cell Biol 1996;16:5069–5080.
28. Kozma R, Sarner S, Ahmed S, Lim L. Rho family GTPases and neuronal growth cone remodelling: Relationship between increased complexity induced by Cdc42Hs. Rac1, and acetylcholine and collapse induced by RhoA and lysophosphatidic acid. Mol Cell Biol 1997;17:1201–1211.
29. Sarner S, Kozma R, Ahmed S, Lim L. Phosphatidylinositol 3-kinase. Cdc42 and Rac1 act downstream of Ras in integrin-dependent neurite outgrowth in N1E-115 neuroblastoma cells. Mol Cell Biol 2000;20:158–172.
30. Ho HY, Rohatgi R, Lebensohn AM, Le M, Li J, Gygi SP, Kirschner MW. Toca-1 mediates Cdc42Dependent actin nucleation by activating the N-WASP-WIP complex. Cell 2004;118:203–216.
31. Bu W, Chou AM, Lim KB, Sudhaharan T, Ahmed S. The Toca-1-N-WASP complex links filopodial formation to endocytosis. J Biol Chem 2009;284:11622–11636.
32. Aurenhammer F. Voronoi Diagrams—A survey of a fundamental geometric data structure. ACM Comput Surv 1991;23:345–405.
33. Aizerman M, Malishevski A. General theory of best variants choice: Some aspects. IEEE Trans Automatic Control 1981;26:1030–1040.
34. Carpenter AE, Jones RT, Lamprecht RM, Clarke C, Kang HI, Friman O, Guertin DA, Chang JH, Lindquist RA, Moffat J, Golland P, Sabatini DM. CellProfiler: image analysis software for identifying and quantifying cell phenotypes. Genome Biol 2006;7: R100. Available at: http://genomebiology.com/2006/7/10/R100.